

Electrical Discharge-assisted Surface Texturing and Coating

ME 315: Supervised Learning Project

Dhruv Sorathiya [200100057]

Shiv Modi [19D100011]

Guide: Prof. Soham Mujumdar



Department of Mechanical Engineering
Indian Institute of Technology Bombay

List of Figures	3
List of Tables	5
Abstract	5
Chapter 1 Introduction	7
1.1 Introduction	7
1.2 Objective	8
1.3 Organization of the Report	9
Chapter 2 Literature Review	10
Chapter 3 Materials and Methods	11
3.1 Sample preparation	11
3.2 Machining Parameter	12
3.3 Circulation System and Flushing	14
Chapter 4 Results and Discussions	16
4.1 Phase 1	16
4.1.1 Discharge Current as variable parameter	16
4.1.1.1 MRR & EWR	16
4.1.1.2 Surface Profile	16
4.1.1.3 Water Contact Angle	19
4.1.2 Pulse On Time Variable	19
4.2 Phase 2	22
4.2.1 Surface Profile	22
4.2.2 Water Contact Angle	24
4.2.3 SEM Analysis	25
Chapter 5 Conclusions & Future Works	29
5.1 Conclusions	29
5.2 Future Work	30
Acknowledgments	31
References	32
Appendix	34

List of Figures

Fig 1.1 EDM phenomena

Fig 1.2 Mechanism of machining and deposition in powder mixed electric discharge machining

Fig 3.1 Workpiece used in phase one(A), tool used in phase one (B), workpiece used n phase two (C), tool used in phase two (D)

Fig 3.2 Snack pattern track

Fig 3.3 machining setup in phase 1

Fig 3.4 Circulation system arrangement

Fig 4.1 a) MRR vs current b) EWR vs current

Fig 4.2 Reference frame orientation and color mapping for surface profiles

Fig 4.3 Variation of a) Surface Roughness - Linear (R_a) , b) Root mean square height (R_q), c) Surface Roughness - Area (S_a), d) Water Contact Angle (WCA) with pulse current (I)

Fig 4.4 Water Drop on EDMed surface for WCA measurement

Fig 4.5 Variation of a) Surface Roughness - Linear (R_a) , b) Root mean square height (R_q), c) Surface Roughness - Area (S_a), d) Material Removal Rate (MRR), e) Electrode Wear Rate (EWR) with pulse on time (T_{on})

Fig 4.6 Surface profiles for a) Workpiece 1, b) Workpeice 2, c) Workpiece 3 and tool path pattern for d) Workpiece 1, e) Workpiece 2, f) Workpiece 3

Fig 4.7 Color mapping for surface profiles a) for 4.6a, 4.6b and 4.6c b) for 4.6d, 4.6e and 4.6f c) reference frame orientation

Fig 4.8 Linear (a) and Area (b) Surafce Roughness variation for all workpieces

Fig 4.9 Water contact angle measurement for a) workpiece 1, b) workpiece 2, c) workpiece 3 by Goniometer

Fig 4.10 Water contact angle plot for workpiece (1), (2) and (3)

Fig. 4.11 SEM images of the workpiece machined with HAp powder(left) and without powder(right)

Fig. 4.12 SEM images of the workpiece machined with HAp powder(left-a) and machined with HAp powder while reusing the dielectric(right-b)

Fig. 4.13 EDS analysis of the machining affected zone (left-a) and EDS analysis of the machining unaffected zone(right-b) on workpiece 1

Fig. 4.14 EDS analysis of the machining affected zone (left-a) and EDS analysis of the machining unaffected zone(right-b) on workpiece 3

Fig. 4.15 EDS analysis of workpiece 2 (machined without HAp powder)

List of Tables

Table 3.1 T_{on} as the varying parameter

Table 3.2 Other constant parameters

Table 3.3 Current varying parameter

Table 3.4 Other constant parameters

Table 3.5 machining parameters in phase two

Table 4.1 Surface Roughness and Surface Profiles with different pulse currents ($I = 4, 14, 24, 32, 48 \text{ A}$)
 $T_{on} = T_{off} = 50 \mu\text{s}$, Voltage = 120 V, Feed Rate = 5 mm/s, Depth of Cut = 0.7 μm , Servo Voltage = 65 V

Table 4.2 Surface Roughness and Surface Profiles with different pulse on time ($T_{on} = 25, 50 \text{ and } 75 \mu\text{s}$),
keeping pulse time period constant ($T = 100 \mu\text{s}$) for $I = 24 \text{ A}$, Voltage = 120 V, Feed Rate = 5 mm/s,
Depth of Cut = 0.7 μm , Servo Voltage = 65 V

Table 4.3 Phase 1 results for Voltage = 120 V, Feed Rate = 5 mm/s, Depth of Cut = 0.7 μm and Servo
Voltage = 65 V

Table 4.4 Elemental distribution of surface machined without powder

Table 4.5 Elemental distribution of surface machined with HAp powder (left-a) and reused dielectric
(right-b)

Abstract

Electrical discharge-assisted surface texturing can modify the surface properties of the metals by varying wettability properties and enhancing corrosion resistance. Such modified surfaces find huge applications in biomedical implants, the chemical industry, and sensing applications. Therefore, electric discharge machining is the most suited method to modify the surface texture to suit the listed applications. In electric discharge machining (EDM), material property modifications occur due to various machining parameters like discharge current, spark gap, voltage, pulse time, duty cycle, etc. The discharge current and pulse on time were found to be the critical parameters for the EDMed surfaces. Surface roughness and the water contact angle on the surface showed an increasing trend as the discharge current increased. Similar findings were also observed for variation of pulse on time keeping the pulse period constant.

One such application on a biocompatible coating using hydroxyapatite has been explored in this work. Stainless steel (SS304) is a widely used biocompatible material due to its mechanical strength and corrosion resistance. However, its prolonged exposure to the corrosion media and long-term biocompatibility is still an issue. Therefore to tackle this issue, a biocompatible coating is required on the surface to reduce SS304 corrosion. For this, a few chemical methods are available, but powder-mixed electric discharge machining using hydroxyapatite and SS304 powder promises a good biocompatible surface. In addition to discharge current and pulse on time, in powder mixed EDM concentration of powders is critical. As a result, this research investigates surface properties modifications of SS304 by performing hydroxyapatite powder mixed EDM (PMEDM) to enhance biocompatibility for medical implants. For analyzing the PMEDM samples, water contact angle measurement for wettability analysis, roughness measurement for surface texture, and FESEM analysis to detect debris, crater, and machined surface morphology have been performed. FESEM analysis shows traces of hydroxyapatite powder on the SS304 substrate. Moreover, to confirm the contamination, FESEM analysis of PMEDM deposited samples has been compared with the normal EDM without powder on the SS304 substrate. Hence, this investigation depicts shreds of the evidence of hydroxyapatite powder deposition on the SS304 substrate by employing PMEDM.

Keywords: **PMEDM; Biocompatible coating; SS304; Hydroxyapatite (HAp)**

Chapter 1 Introduction

1.1 Introduction

Stainless steel is widely used in industry and daily human life. It is a very useful material due to its corrosion resistance and strength properties. Stainless steel also has potential applications due to its surface properties. Applications include the biomedical industry. Millions of people need implants for the replacement of broken bones in accidents. To fulfill such a huge task, it's essential to make the manufacturing process precise and effective. While it is possible to machine 304 steel using conventional fabrication techniques such as CNC lathe, CNC milling, shaping, boring, and turning, these operations cannot guarantee recast layer and biological reactions. The surface of biomaterials is now coated using various surface modification techniques, such as physical and chemical deposition methods. However, these surface modification techniques cannot provide changed surfaces with narrow nanopores and strong coating adherence. Additionally, the specimens must be prepared using these techniques beforehand, increasing the final output cost. The nontraditional technique called electrical discharge process (EDM), which was introduced in industrial applications in the mid-19th century, enables to machine and coat the biomaterials' surface concurrently.

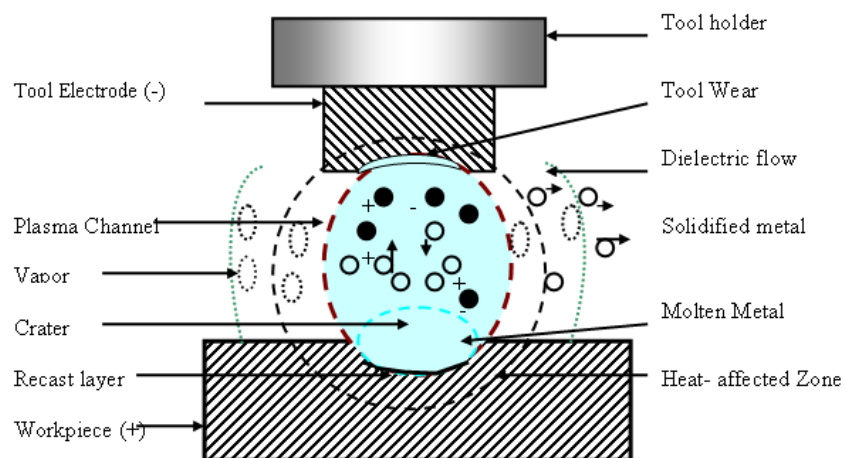


Fig 1.1 EDM phenomena [1]

The particular one used for this project is die-sinking EDM with EDM oil (hydrocarbon oil) as the dielectric. When a voltage is applied between a tool and workpiece, a dielectric discharge occurs, bringing them close to each other with a minute spark gap. Due to this phenomenon, plasma formation occurs in the region between the tool and the workpiece, creating a very high temperature that leads to material removal from the workpiece. Since this material removal mechanism involves melting and evaporation, the hardness of the material is not of concern anymore. In the process of material removal, the machining parameters are very critical, and they need to be tuned well to get the desired surface characteristics. The variation of material removal rate, electrode wear rate, the surface roughness of the workpiece, machining

time, wettability properties, and many others have been extensively studied by many people worldwide. Properties taken into consideration by us are further discussed in the objective section.

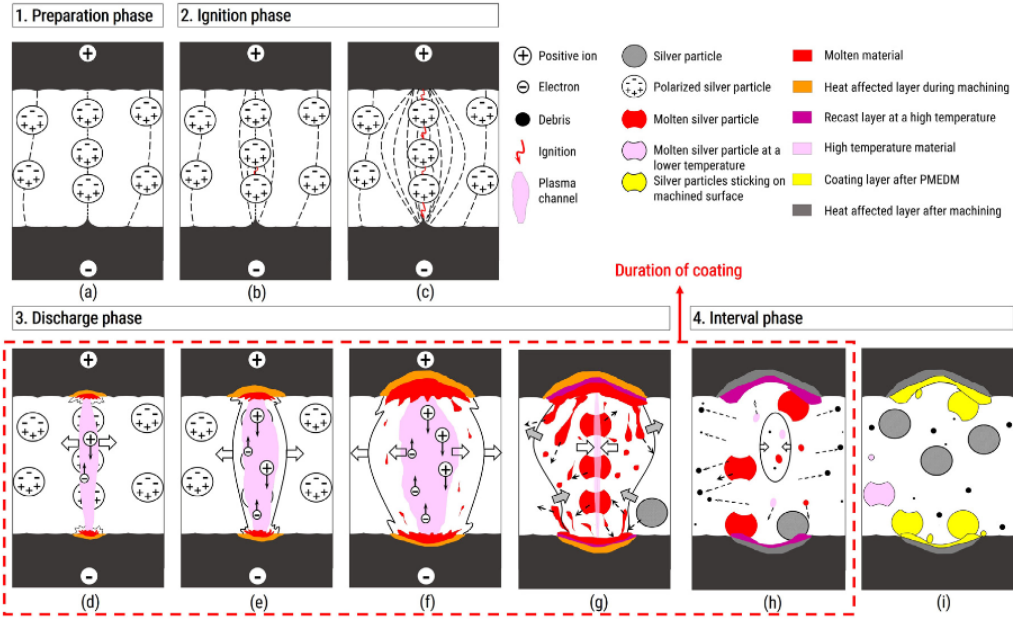


Fig. 1.2 Mechanism of machining and deposition in powder mixed electric discharge machining[2]

One more critical aspect of the die-sinking EDM is that it can coat the powder material on the surface of the workpieces. It can do the workpiece's material removal and coat the powder simultaneously. The addition of conductive particles increases the sparking, leading to an increase in the spark gap. So the discharge becomes easier. Once the plasma formation is done and the material is removed during the pulse-on period, material debris, along with the powder particles, settles on the surface of the workpiece. This phenomenon is called recasting and deposition of the powder and can be visually seen in figure 1.2. Literature validates the proper adhesion of the powder on the surface. This area of EDM machines has been explored in this project. The report includes all the literature review conclusions and results obtained by our experiments.

1.2 Objective

This project has been divided into two phases; in the first phase, our focus was on studying the wetting properties, Material Removal Rate(MRR), Electrode Wear Rate (EWR), and surface topology of the EDMed surface. Pulse properties and the current were chosen as varying parameters.

While in the project's second phase, our focus was to generate biocompatibility on the surface of SS304 by coating it with hydroxyapatite (HAp) and silver(Ag) powder. Both the powders have shown biocompatibility. The objective was to study the variation of surface texture properties with the machining parameters concentration of powders, current, and feed rate. Further discussion and analysis are included in the following sections.

1.3 Organization of the Report

Chapter 2: Literature review

This section contains the literature review done for phases one and two. It extensively contains all the literature and their interpretation for our project.

Chapter 3: Materials and Methods

This chapter includes the entire procedure of the conduction and analysis of the experiments in phases one and two. Based on the design of experiments made from the literature, tables of machining parameters are included in the section. Details of all the equipment used can be found in the section.

Chapter 4: Results and Discussions

This section includes the results obtained from the analysis of the textured surfaces. Analysis and interpretation of various topographical parameters, wetting properties, and elemental distribution analysis are included in the section. Additionally, trends of material removal rate and electrode wear rate are also included.

Chapter 5: Conclusions

The final section contains conclusions based on the results obtained.

Chapter 2 Literature Review

Electric discharge-assisted surface texturing can generate different wetting and corrosion properties on the surface of SS304. Different surface-wetting characteristics find different applications. Superhydrophobic surfaces have been considered for sensing applications such as thermal and pH sensors [3] Bioinspired surfaces are made to generate hydrophobicity through various surface textures [4]. Wetting properties have a correlation with surface topographical properties, the water contact angle increases as roughness increases[5]. The surface roughness value decreases with the increase in spark gap [6]. A paper has found that pulse current, discharge time, and the interaction term of pulse current with other parameters significantly affect surface roughness. Surface roughness is directly proportional to the linear effect of pulse current, and pulse on time current and pulse on time are the machining parameters that affect the roughness of the surface [7]. On increasing the current and pulse on time, keeping the other parameters constant, roughness increases, and so does the water contact angle [5, 9-11]. The effect of these machining parameters on the material removal rate and electrode wear rate is also important. MRR increases with the increase in current and pulse on time [5, 9, 10].

After reconsidering the novelty aspect of the work, we reviewed the literature again on applications of EDM textured surfaces. We found a significant novelty in the field of powder-mixed electric discharge machining. Coating various powders on stainless steel is very effective from an applications point of view. A paper has mentioned biomedical applications of HAp[6], and graphite-coated SS316L alloy and a few more applications in nuclear reactors, the food industry, and hydro turbines [8]. They can increase the biocompatibility of the implants. A review paper [11] has found that hydroxyapatite powder brings biocompatibility to the surface of the steel. Hydroxyapatite is $\text{Ca}_{10}(\text{PO}_4)_6(\text{OH})_2$. It contains calcium phosphates similar to the bones' composition, which introduces the implants' biocompatible nature. When this powder is added to the dielectric in a specific concentration, it induces biocompatibility. A high calcium-phosphorous proportion in the formed coating can enhance osteoblast adhesion development more [12]. Since pores increase the surface contact area of the bio-implant, surface roughness associated with pores develops a strong relationship between the bio-implant surface and the hard tissue to improve osteointegration, osteoinduction, cell adhesion, protein adsorption, bone-like apatite formation, and ions exchange. According to published research, SR at microscales between 0.4 and 7.4 μm ensures excellent biological responses. Recently, it has been determined that the ideal surface condition for cell adhesion and osteoinduction is nano-scale roughness ($100 \text{ nm} < \text{SR} < 1 \mu\text{m}$). Additionally, because of the decreased friction coefficient, the nano-scale roughness reduces the relative friction between the coating and bone, contributing to the coating's high durability. [13-16]. Proteins and physiological fluids surround the implant surfaces. Therefore, their hydrophilicity and surface energy are crucial for the attachment of cells. Additionally, the biological response, which affects how biocompatible a material is, is significantly influenced by surface hydrophilicity. It greatly depends on the surface energy, surface roughness, and surface topography of the biomaterials. [17-19].

Chapter 3 Materials and Methods

This section describes the methodologies used to perform the machining and for the derivation of the results. Modifications were done in the original setup of the EDM machine when powder-mixed EDM was performed, all the details are included in the following section.

3.1 Sample preparation

The material of interest for the experiments was Stainless Steel 304. It is the most versatile and widely used type of steel. It contains 18% Chromium and 8% nickel, and a very minute amount of carbon. In phase one, the dimension of each workpiece was **6.5cm×3cm**, and the thickness was **8mm**. The electrode used in the experiment was copper, with a cross-section area of **16mm×16mm**. Three machining patches were made on each of the workpieces. The below figure shows the polished workpiece before machining.

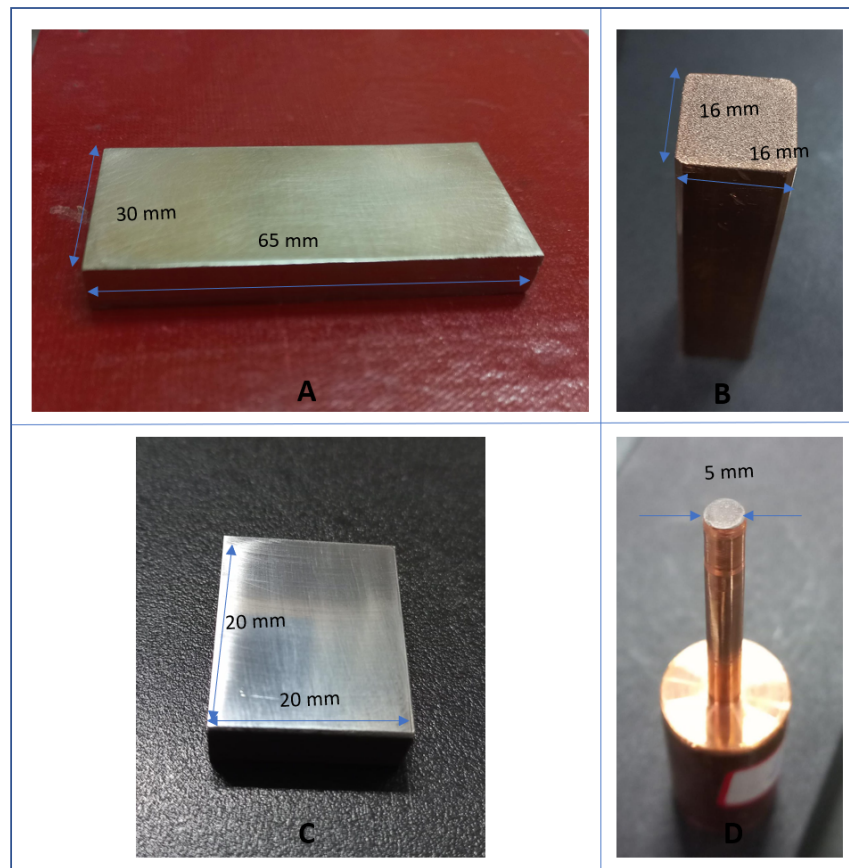


Fig 3.1 Workpiece used in phase one(A), tool used in phase one (B), workpiece used n phase two(C), tool used in phase two(D)

While in the second phase, the dimension of each workpiece was **2cm×2.4cm**, and the thickness was **again 8mm**. The electrode used in the experiment was copper with a **5mm** diameter. The diameter of the tool was kept 20 mm to make mounting it easier on the machine.

Workpieces were cut by wire EDM to give the specific dimensions and were surface milled and polished through 150, 300, 600, 800, 100, 1500, and 2500 grade sandpapers sequentially to make the surface smooth and uniform for the machining. The electrode also needed to be polished after each experiment to maintain the uniformity and consistency of roughness of the electrode surface for multiple experiments. To determine the material removal rate and the tool wear rate of the workpieces, they were weighed before and after the machining for each workpiece and the tool. The weighing machine had the least count of one milligram; this much of the least count is needed since the amount of material being removed is quite small. Along with that, the machining time was also united.

In the first phase, machining was done by feeding the workpiece in a vertically downward direction while keeping the X-Y position constant. A depth of 0.7mm was given. In this case, we cannot control the vertical feed rate since the machine automatically controls it. It moves the tool in a downward direction as the material gets removed.

3.2 Machining Parameter

In phase 1, varying machining parameters chosen were current and pulse properties. 5 levels of current for constant pulse on and off times were experimented with. And with a given constant current, 3 levels on time were experimented on while keeping the total pulse period constant as 100 **μs**. A few preliminary experiments were conducted, and then, according to the literature review, the below design of the experiment was finalized.

Table 3.1 T_{on} as the varying parameter

Parameter	Level 1	Level 2	Level 3
T_{on}	25 μs	50 μs	75 μs
T_{off}	75 μs	50 μs	25 μs

Table 3.2 Other constant parameters

Parameter	Specification
Voltage	120 V
Servo voltage	65 V
Discharge current	24A
Depth of cut	0.7mm

Table 3.3 Current varying parameter

Parameter	Level 1	Level 2	Level 3	Level 4	Level 5
I	4 A	14 A	24 A	32 A	48 A

Table 3.4 Other constant parameters

Parameter	Specification
Voltage	120 V
Servo voltage	65 V
Discharge current	24A
Pulse on time	50 us
Pulse off time	50 us

While in the second phase of the project, Method was changed to a snack pattern. Keeping the same 0.1mm depth of cut in the z-direction, the tool was given a feed in the X-Y plane to cover the patch of **20mm×20mm** in a snack-like pattern as given in fig.3.2.

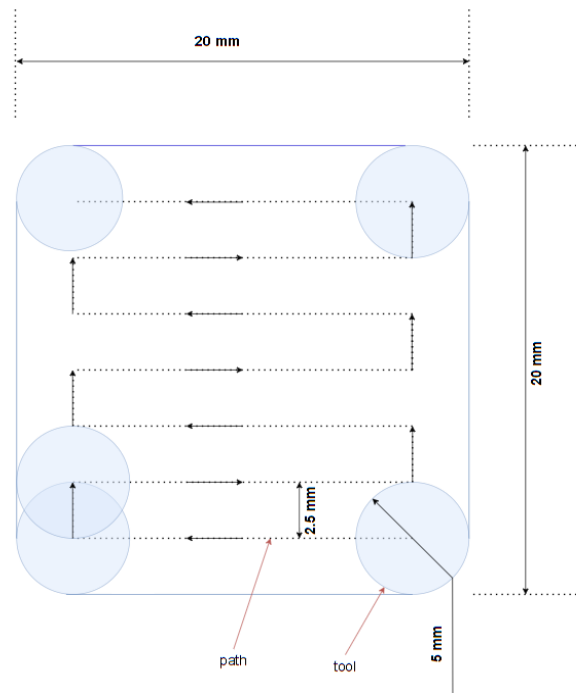


Fig. 3.2 Snack pattern track

3.3 Circulation System and Flushing

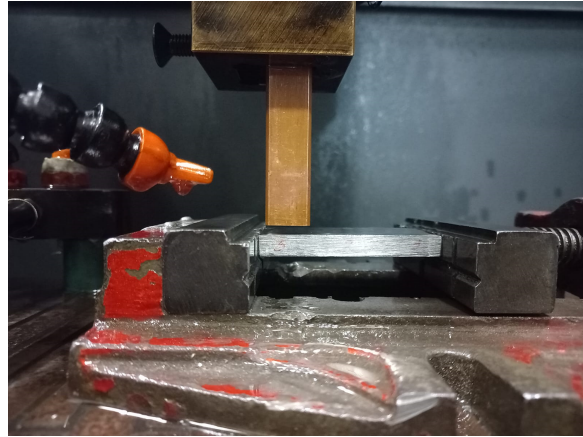


Fig.3.3 machining setup in phase 1

One important aspect in the second phase was the circulation system. The addition of powder in the main dielectric circulation tank is not desired as it may clog the filters inside the machine, and it might also lead to wastage of the dielectric since we might not have a proper method to separate the powder from the dielectric fluid. A separate tank of approximate dimensions **400mm×240mm×150mm** was made using plastic sheets to solve the issue. A laser cutter was used to cut the plate in such a way that all the vertical plates could be assembled with the base plate easily.

A submersible pump was used to circulate the powder-mixed dielectric. It was placed inside the tank, as visible in Figure 3.3. Two coolant pipes were directly connected to the pump, flushing the jet of dielectric on the workpiece. The main flushing system of the machine was turned off, and the level up to which dielectric fill in the main tank of the machine was set at the lowest level to avoid redundancies.

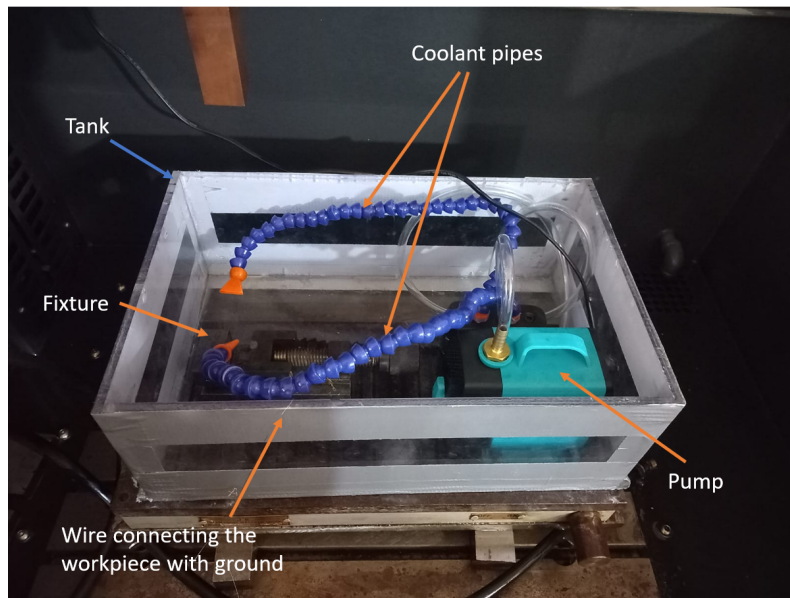


Fig.3.4 Circulation system arrangement

In phase two, a total of three samples were machined. One with a 2.5 g/L concentration of hydroxyapatite powder added to a dielectric of 10L volume. The second workpiece was machined without powder, keeping the other machining parameters constant. The third workpiece was machined, resuing the dielectric left after machining the first workpiece to study the reusability of the dielectric.

Table 3.5 Machining parameters in phase two

Parameter	Specification
Discharge Current	14 A
Voltage	120 V
Servo voltage	65 V
Pulse on time	50 us
Pulse off time	50 us
Feed rate	1 mm/s

To perform the analysis of surface topography, Bruker ALICONA μ CMM machine was used in Machine Tools Laboratory. The 10X magnification lens was used while scanning the surface for roughness measurements. For the analysis of the wetting properties, a GBX digit drop goniometer was used; this equipment is present in the PG lab, chemical department. And for the analysis of the elemental distribution of the machined workpieces, FESEM-EDS was used by the MEMS department.

Chapter 4 Results and Discussions

This chapter discusses the results obtained during both project phases. Results of phase one include an analysis of the water contact angle and surface topography. In contrast, the second phase results include the analysis of the water contact angle, surface topography, and elemental distribution analysis.

4.1 Phase 1

In the first phase of the experiment, we examine the effect of two parameters, current and pulse on time.

4.1.1 Discharge Current as variable parameter

4.1.1.1 MRR & EWR

One important parameter analyzed was the Material Removal Rate which signifies how fast the manufacturing process is. An increasing trend was found for MRR with the current as seen in Fig 4.1a. It increases gradually up to the current of 32A while there is a drastic increase in MRR for the 48A current.

Measurement and study of Electrode Wear Rate also play an important role since it highly affects the industrial economy. Higher EWR can lead to very frequent breaking of tools and it becomes economically expensive. The trend obtained for the parameter is similar to the trend of MRR. It increases as the current is increased. And there is a huge relative change in EWR at the current of 48 A, as seen in Fig 4.1b.

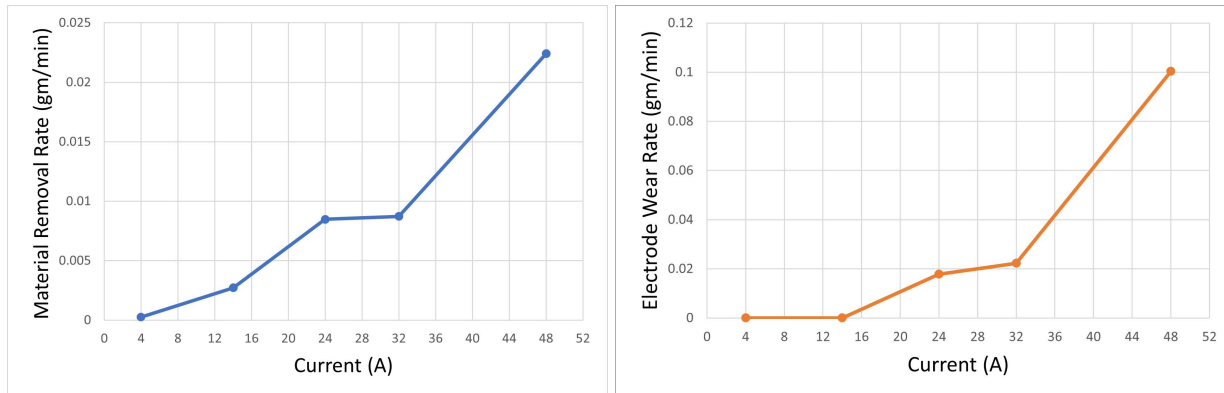


Fig. 4.1 a) MRR vs current b) EWR vs current

4.1.1.2 Surface Profile

Different surfaces obtained from the current variation are shown in Table 4.1 with parameters. Colored images in the table make it easy to visualize the surface profile. The scale for the colours is given in Figure 4.2. The profiles show that non-uniformness increases with the current value. Peak heights and valley depths also increase with the discharge current since the discharge energy is high and the amount of material being removed is also high in the given amount of time.

Table 4.1 Surface Roughness and Surface Profiles with different pulse currents (I = 4, 14, 24, 32, 48 A)
 $T_{on} = T_{off} = 50 \mu\text{s}$, Voltage = 120 V, Feed Rate = 5 mm/s, Depth of Cut = 0.7 μm , Servo Voltage = 65 V

Pulse Current (A)	Surface Roughness (μm)	Profile
4	0.9964	
14	1.1992	
24	1.05598	
32	2.3684	
48	1.3700	

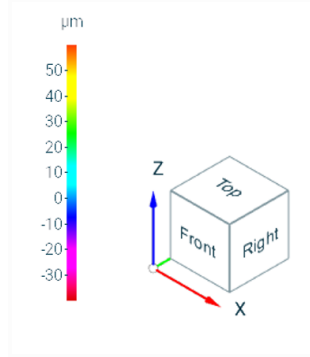


Fig 4.2 Reference frame orientation and color mapping for surface profiles

Surface roughness (R_a) (also called Arithmetic Mean Height) and Root Mean Square height (R_q) increase first and then decrease while area-wise surface roughness (S_a) overall increase with discharge current as shown in Fig 4.3a, 4.3b and 4.3c. This behavior can be explained as the greater pulse current will generate higher energy to melt and evaporate the material. Eventually, it will cause a thicker recast layer, which will result in high surface roughness (R_a) and material removal rate (MRR) or electrode wear rate (EWR) [17].

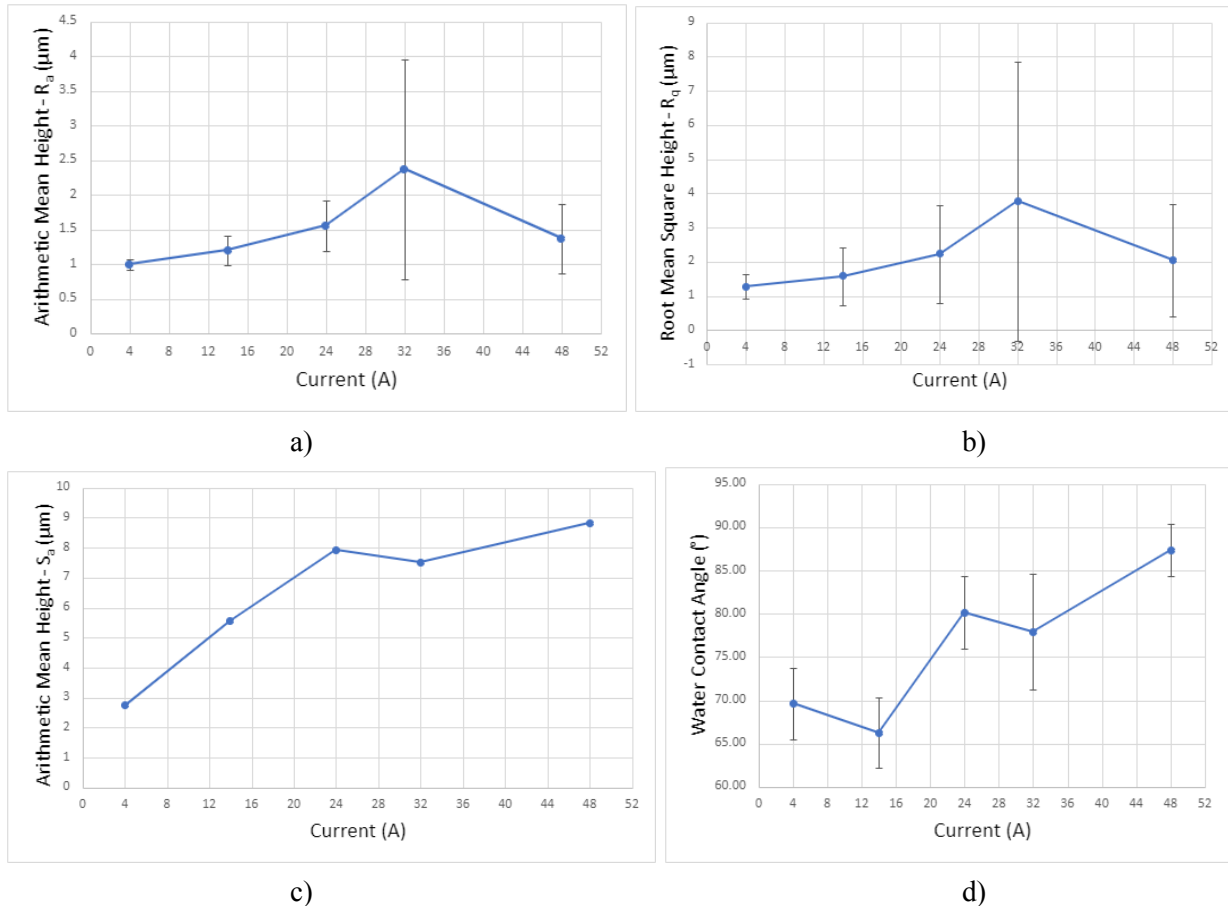


Fig 4.3 Variation of a) Surface Roughness - Linear (R_a), b) Root mean square height (R_q), c) Surface Roughness - Area (S_a), d) Water Contact Angle (WCA) with pulse current (I)

4.1.1.3 Water Contact Angle

Water contact angles as pulse current varied shown in Fig 4.3d. WCA overall increases in a zigzag manner with increasing pulse current, which can be explained by surface roughness variation with pulse current. Literature shows that WCA directly depends on surface roughness and increase of surface roughness results in increase of WCA with pulse current.

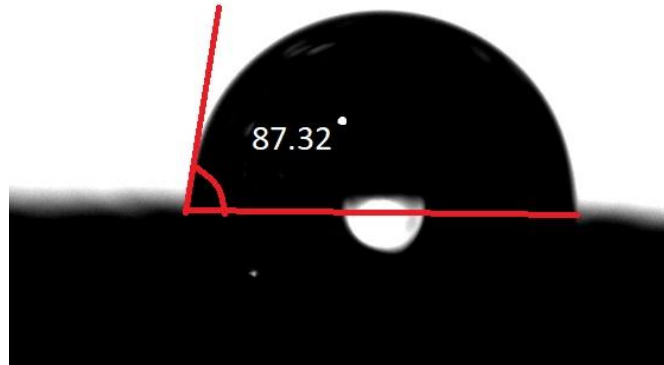


Fig 4.4 Water Drop on EDMed surface for WCA measurement

4.1.2 Pulse On Time Variable

In next step, surface profiles are generated by varying pulse on time (T_{on}) keeping pulse time period same. Surfaces obtained from pulse on time variation shown in Table 4.2. As shown, increase of pulse on time will result in non-uniformness and increase of peak heights and valley depths.

Plots of surface roughness (R_a), root mean square height (R_q), area wise surface roughness (S_a), material removal rate (MRR) and electrode wear rate (EWR) varied with pulse on time shown in Fig 4.5a, 4.5b, 4.5c, 4.5d and 4.5e. The greater of T_{on} will cause the greater of heat absorbed by the material, which will cause the greater of material removal rate (MRR), so it will produce more debris. The presence of debris will cause the surface rougher, and the recast layer is thicker. If the T_{on} is greater, then the melting and evaporation of the workpiece will be greater. The greater melting and evaporation of the workpiece occur due to the high amount of heat absorbed by the material, and it will reduce the flushing efficiency. [17] The above phenomenon will cause the recast layer thicker, and explains why values of area surface roughness and MRR increases in plots varies with pulse on time. Here surface roughness (R_a) and root mean square height (R_q) first increase and then decrease with pulse on time. Also, results shows that EWR decreases with increase of T_{on} .

Table 4.2 Surface Roughness and Surface Profiles with different pulse on time ($T_{on} = 25, 50$ and $75 \mu\text{s}$), keeping pulse time period constant ($T = 100 \mu\text{s}$) for $I = 24 \text{ A}$, Voltage = 120 V, Feed Rate = 5 mm/s, Depth of Cut = 0.7 μm , Servo Voltage = 65 V

Pulse On Time (μs)	Pulse Off Time (μs)	Surface Roughness (μm)	Profile
25	75	1.0074	
50	50	1.05598	
75	25	1.1834	

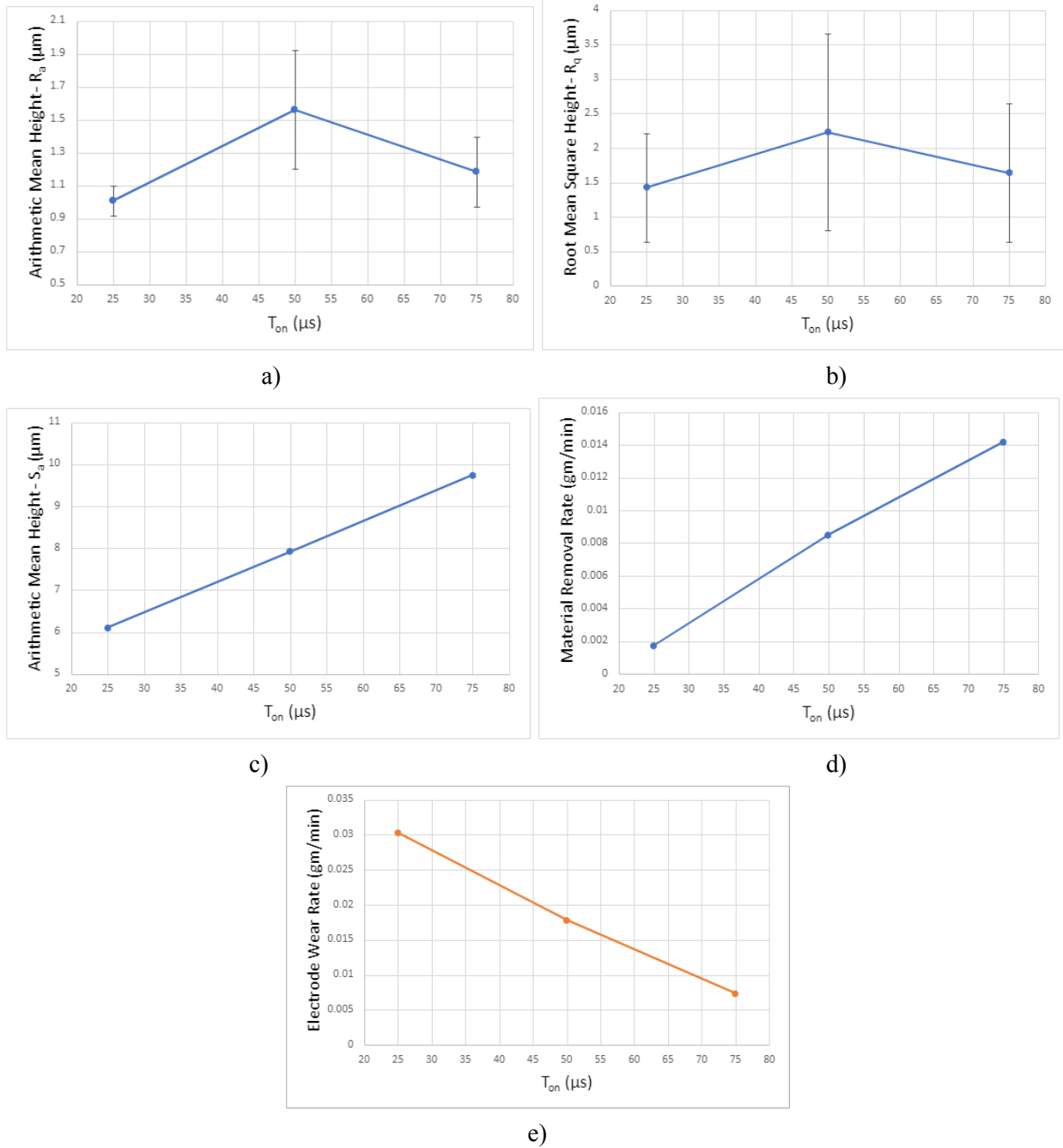


Fig 4.5 Variation of a) Surface Roughness - Linear (R_a), b) Root mean square height (R_q), c) Surface Roughness - Area (S_a), d) Material Removal Rate (MRR), e) Electrode Wear Rate (EWR) with pulse on time (T_{on})

Table 4.3 Phase 1 results

For Voltage = 120 V, Feed Rate = 5 mm/s, Depth of Cut = 0.7 μm and Servo Voltage = 65 V

Current (A)	4	14	24	32	48	24	24
T _{on} (μs)	50	50	50	50	50	25	75
T _{off} (μs)	50	50	50	50	50	75	25
Energy (mJ)	24	84	144	192	288	72	216
MRR (gm/min)	0.00026	0.00272	0.00848	0.00873	0.0224	0.00174	0.01417
EWR (gm/min)	0.00002	0.00006	0.01787	0.02229	0.1004	0.03037	0.00737
S _a (μm)	2.745	5.562	7.919	7.527	8.834	6.102	9.732
S _q (μm)	3.406	7.016	10.428	10.044	11.402	7.952	12.596
S _z (μm)	50.256	69.207	98.543	87.396	80.96	63.105	106.822
S _{sk}	-0.298	0.475	0.607	0.814	0.575	0.698	0.666
S _{ku}	2.887	3.143	4.564	4.708	3.71	4.084	3.763
S _{dq}	0.445	0.538	0.697	0.931	0.703	0.512	0.744
S _{dr} (%)	8.878	13.203	20.206	31.868	20.487	11.365	23.351
WCA (Degree)	69.65	66.26	80.12	77.92	87.33	73.67	
R _a (μm)	0.9964	1.1992	1.5598	2.3684	1.37	1.0074	1.1834
R _q (μm)	1.28	1.586	2.233	3.777	2.048	1.429	1.642

4.2 Phase 2

In phase 2, a total of 3 workpieces were experimented as following conditions:

- Workpiece 1: Hydroxyapatite (HAp) Powder Mixed EDM
- Workpiece 2: Conventional EDM (No powder mixed)
- Workpiece 3: Reused Powder - Mixed EDM Oil of workpiece 1

Other EDM parameters for all experiments were same as shown in Table 3.5.

4.2.1 Surface Profile

PMEDMed workpiece has more non uniformness than normal EDMed workpiece. Resued PMEDM OIl increases uniformness even more then normal EMDed workpiece. (Fig 4.6a, 4.6b and 4.6c). In Fig 4.6d, 4.6e and 4.6f, border of tool path is clearly visible, because there is possibility of spark escape from edge of tool of circular cross section to nearby area.

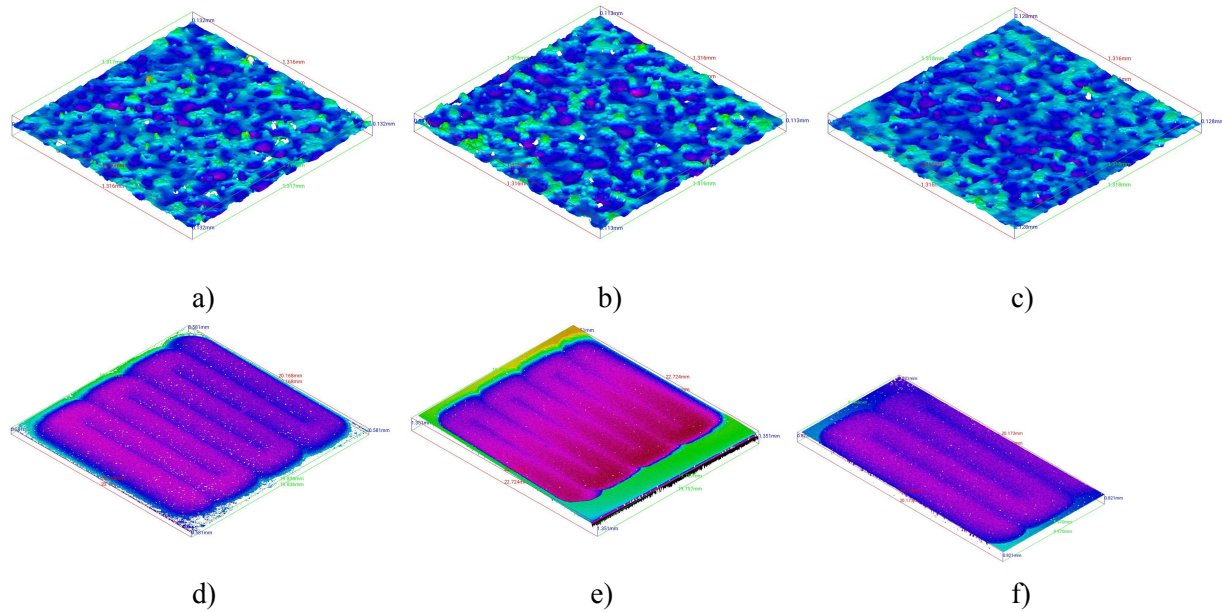


Fig 4.6 Surface profiles for a) Workpiece 1, b) Workpiece 2, c) Workpiece 3 and tool path pattern for d) Workpiece 1, e) Workpiece 2, f) Workpiece 3

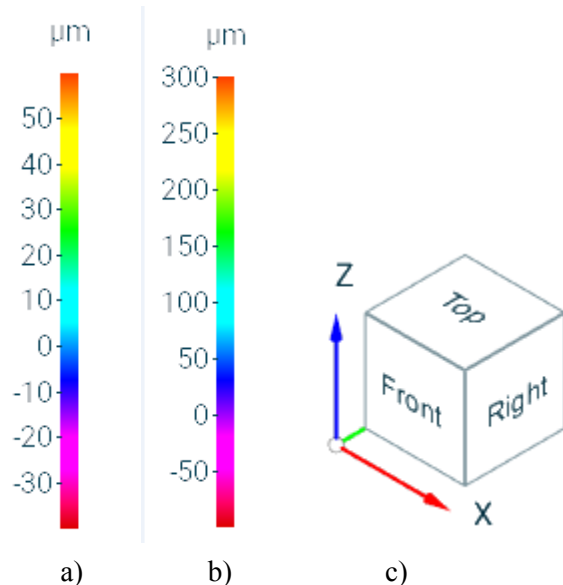
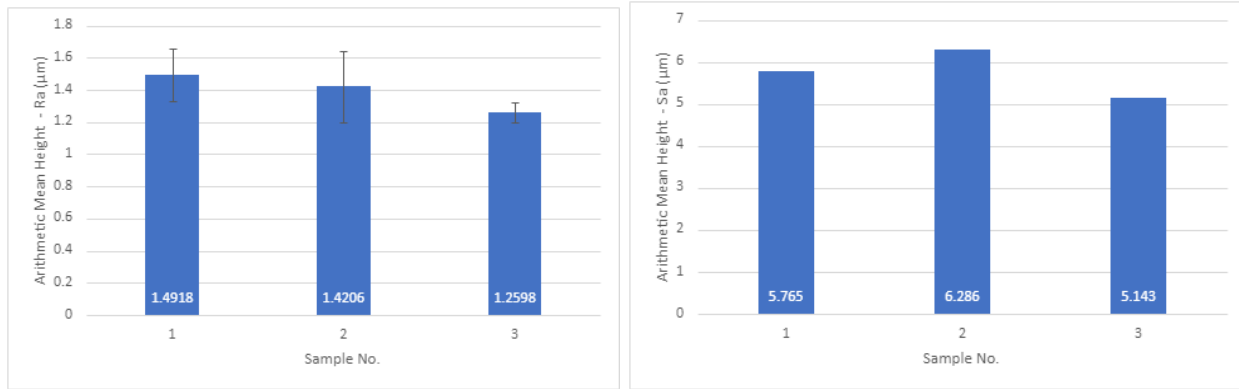


Fig 4.7 Color mapping for surface profiles a) for 4.6a, 4.6b and 4.6c b) for 4.6d, 4.6e and 4.6f c) reference frame orientation

Linear surface roughness (R_a) of PMEDM workpiece is higher than normal EDM workpiece. Also, workpiece fabricated with reused PMEDM Oil posses lower surface roughness than normal EDM workpiece. (Fig 4.8a). Normal EDM workpiece has highest areal surface roughness (S_a) than PMEDM workpiece and workpiece fabricated with resued PMEDM Oil. Although reusing PMEDM Oil result decrease in areal sarface roughness. (Fig 4.8b)



a)

b)

Fig 4.8 Linear (a) and Area (b) Surface Roughness variation for all workpieces

4.2.2 Water Contact Angle

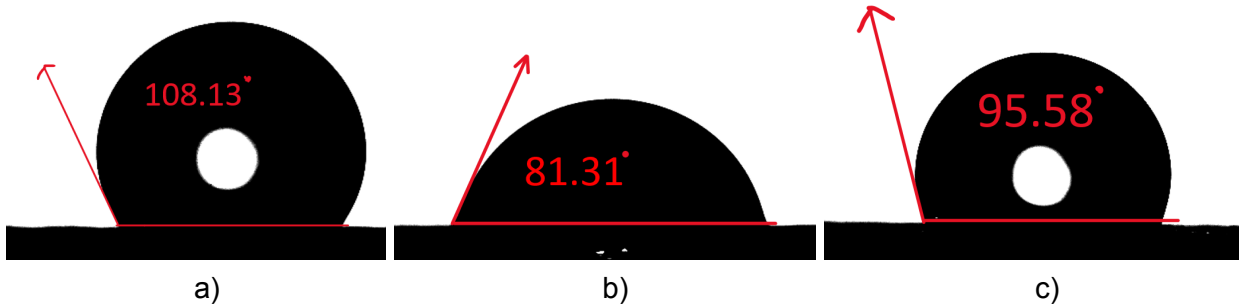


Fig 4.9 Water contact angle measurement for a) workpiece 1, b) workpiece 2, c) workpiece 3 by Goniometer

Water Contact Angle (WCA) of the PMEDMed workpiece is higher than normal EDMed workpiece. Also, reusing PMEDM Oil results decrease in WCA, but this value is still higher than the workpiece fabricated through normal EDM. (Fig 4.10)

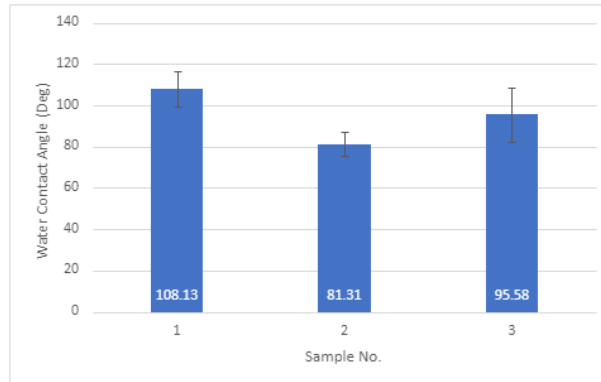


Fig 4.10 Water contact angle plot for workpieces (1), (2), and (3)

4.2.3 SEM Analysis

All three phase two samples were analyzed using FESEM-EDS to determine the elemental distribution and thus verify powder deposition. Detailed graphics and analysis is given as follows in this section.

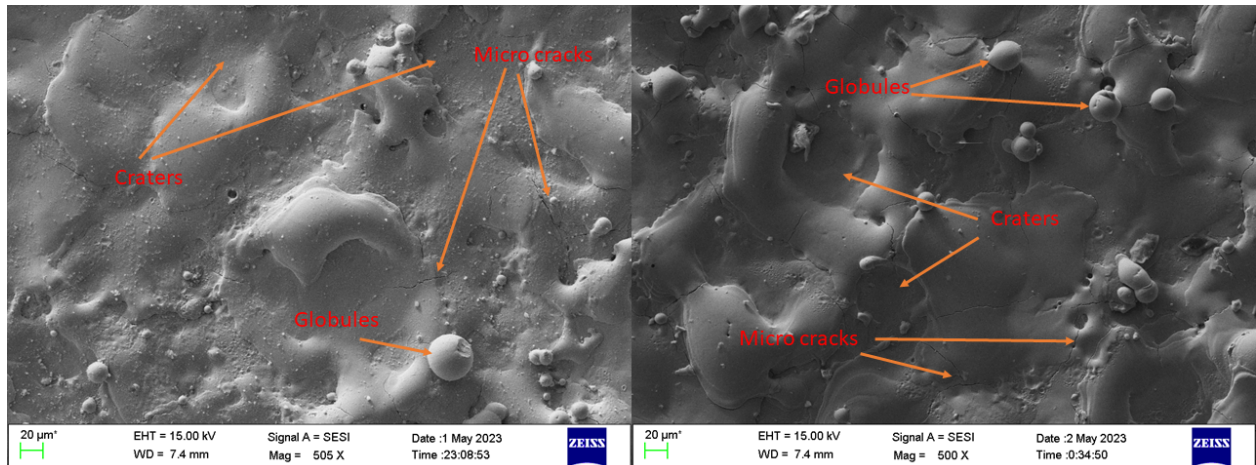


Fig. 4.11 SEM images of the workpiece machined with HAp powder (left) and without powder (right)

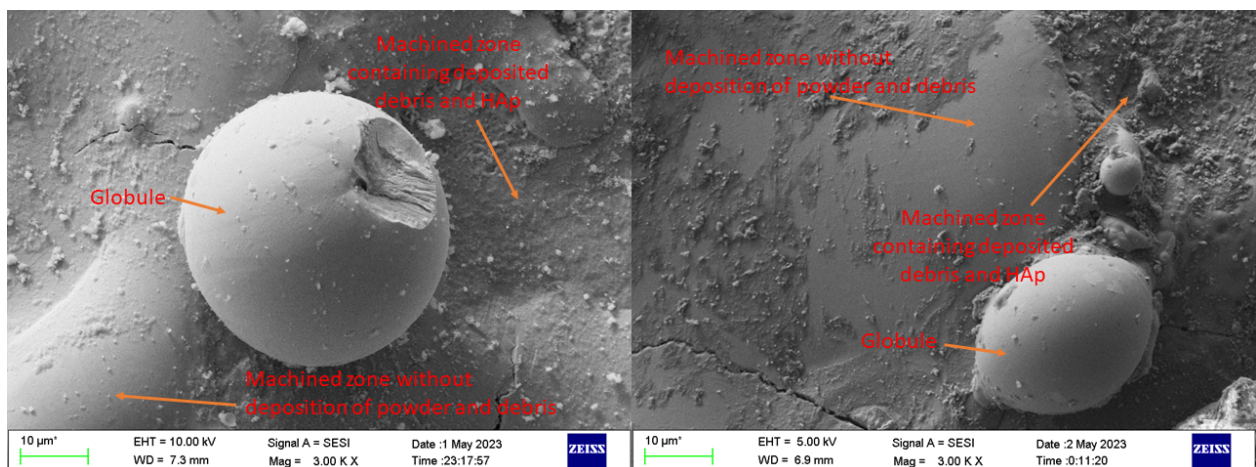


Fig. 4.12 SEM images of the workpiece machined with HAp powder(left-a) and machined with HAp powder while reusing the dielectric(right-b)

In the above images taken with SEM at 500x magnification, craters, globules, debris, and microcracks are clearly visible. The amount of debris and powder deposition is significant in image 1 (with powder), while in the second image, since the workpiece was in the main flushing tank, no debris is present. Fig 4.12 contains the images taken at 3000x, they show the similarities present in workpieces 1 and 2. They both have identical debris, powder deposition, and the unaffected zone where the surface did not go under sparking. This clearly suggests that resuing the dielectric can regenerate a similar texture on the new workpiece.

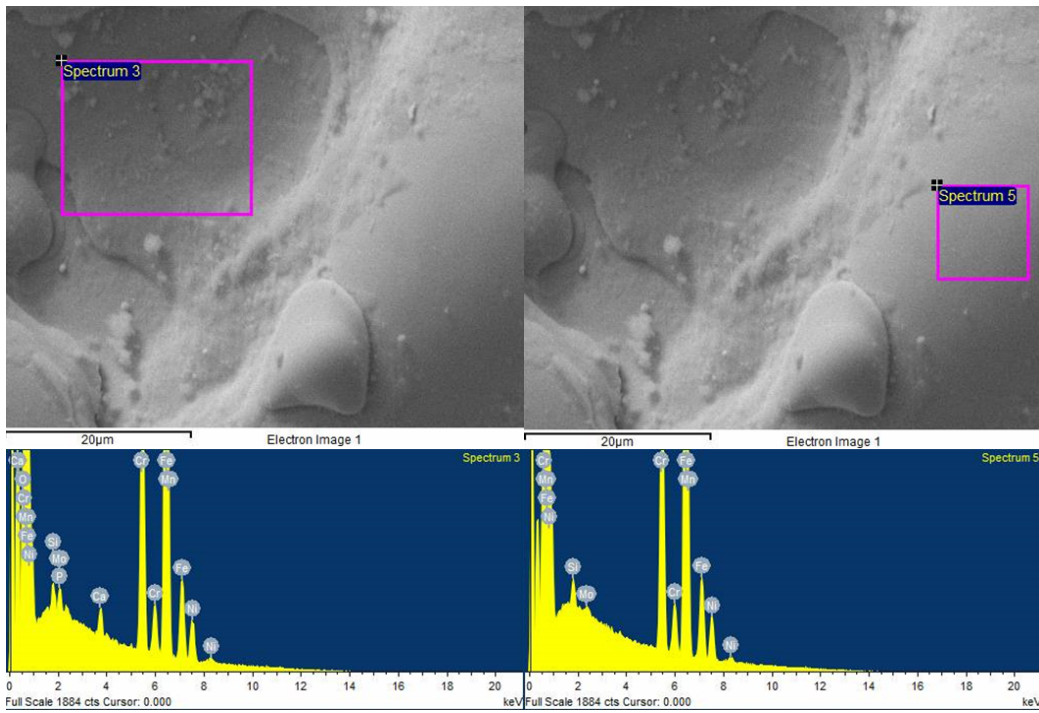


Fig. 4.13 EDS analysis of the machining affected zone (left-a) and EDS analysis of the machining unaffected zone(right-b) on the workpiece 1

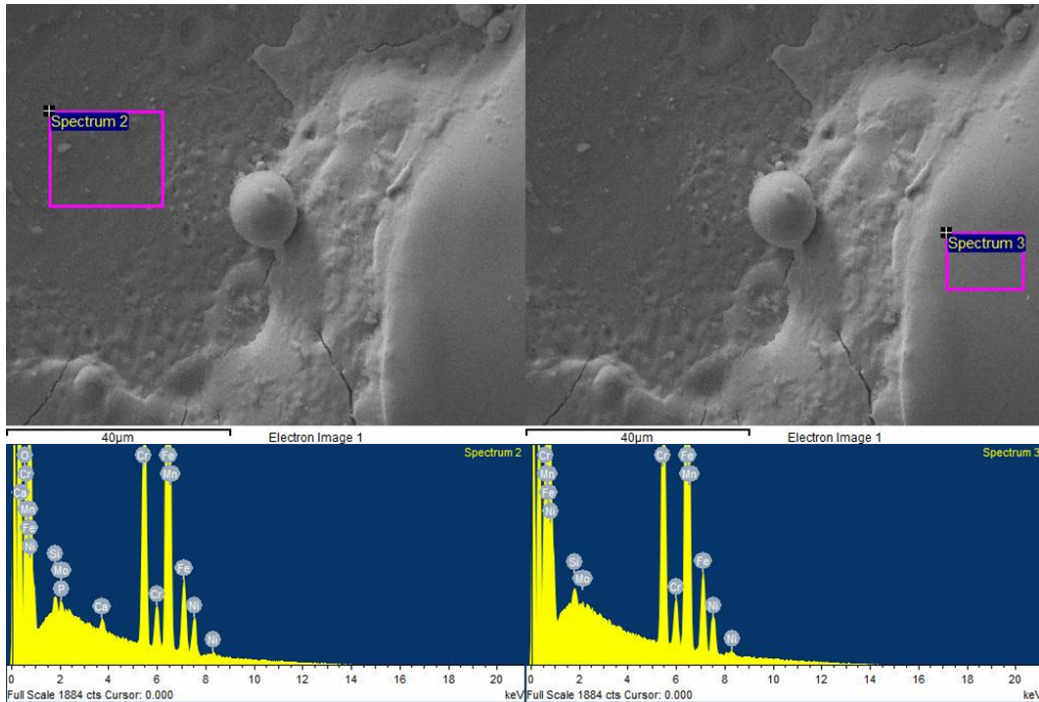


Fig. 4.14 EDS analysis of the machining affected zone (left-a) and EDS analysis of the machining unaffected zone(right-b) on workpiece 3

EDS characterization was done to identify the elemental distribution of all the surfaces. On workpiece 1 which was machined with HAp powder, the presence of hydroxyapatite was confirmed due

to the presence of phosphorus and calcium elements as seen in Fig 4.14a. While in the machining unaffected zone of the same workpiece, neither P nor Ca was found as seen in Fig 4.14b. Similar results were obtained for the 3rd workpiece 1 which dielectric was reused as seen in Fig 4.14a.

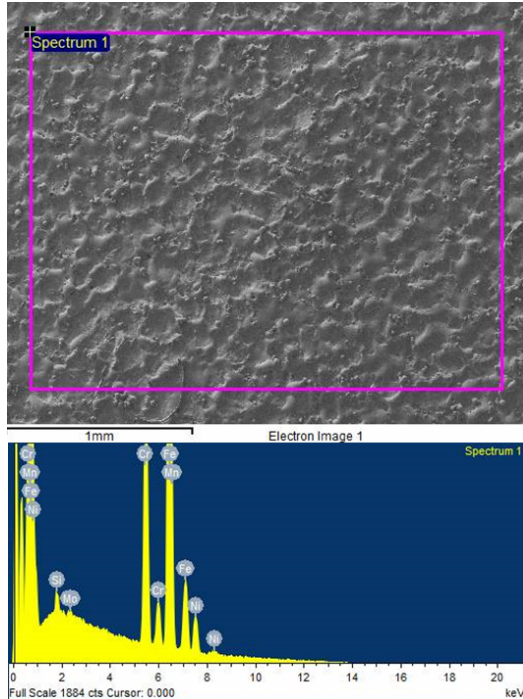


Fig. 4.15 EDS analysis of workpiece 2 (machined without HAp powder)

While in the EDS analysis of the surface machined without HAp powder, the resultant spectrum was obtained, as seen in Fig 4.15. In all the above spectrum Figures, it can be seen that the majority of the amount present are the basic elements of the stainless steel 304, which are Iron, Chromium, Nickel, and Manganese. While elements like Silicon and Oxygen are present on the surface due to impurities. A small amount of molybdenum was also found in every region of the workpieces.

In the elemental distribution of the workpiece machined without powder, the components obtained were the fundamental components of the stainless steel 304, individual weight percentages are given in Table 4.4. While in the other two workpieces, both the elements Calcium and Phosphorus were found. Ca to P ratio has been found critical according to the literature [11] and there is a standard value of 1.6, which is required in order to achieve biocompatibility. Workpiece one has Ca to P ratio of 1.58 and workpiece three has Ca to P ratio 1.5. Which are very close to 1.6 and it supports biocompatibility. While one observation that can be drawn from these results is that the percentage weight has reduced in when the dielectric was reused. That is due to the fact that some amount of powder couldn't be recollected in to the container because it settled down. This led to a reduction in concentration and, thus the reduction in percentage weight of the Calcium and phosphorous on the coated surface.

Table 4.4 Elemental distribution of surface machined without powder

Element	Weight%	Atomic%
Si K	0.53	1.04
Cr K	19.31	20.44
Mn K	1.34	1.34
Fe K	70.71	69.70
Ni K	7.77	7.29
Mo L	0.34	0.19
Totals	100.00	

Table 4.5 Elemental distribution of surface machined with HAp powder(left-a) and reused dielectric(right-b)

Element	Weight%	Atomic%
O K	4.44	13.71
Si K	0.52	0.92
PK	0.38	0.61
Ca K	0.60	0.75
Cr K	18.29	17.39
Mn K	1.24	1.11
Fe K	66.73	59.07
Ni K	7.41	6.24
Mo L	0.39	0.20
Totals	100.00	

Element	Weight%	Atomic%
O K	4.55	14.04
Si K	0.62	1.09
PK	0.28	0.44
Ca K	0.42	0.52
Cr K	18.50	17.56
Mn K	1.10	0.99
Fe K	66.80	59.01
Ni K	7.29	6.12
Mo L	0.43	0.22
Totals	100.00	

The above SEM analysis shows the deposition of hydroxyapatite has occurred as per the requirement. Further conclusions based on those results are added in the following section.

Chapter 5 Conclusions & Future Works

5.1 Conclusions

Phase 1: Machining of SS304 using a copper electrode of cross-section 16mm×16mm and 0.7mm depth of cut with feed given only in z-direction

- Current as a varying parameter, values: [4 A, 14 A, 24 A, 32 A, 48 A]
 - MRR and EWR increase with the increase in current
 - Surface roughness parameter R_a increases with the increase in current, but there is a slight deviation in the trend for 48 A current. The roughness value at 48 A current is lower than that of 32 A
 - R_q values also show similar trends to that of R_a , which increases with an increase in current but deviation from the trend for 48 A current
 - S_a values increases with an increase in current, while one exception is at 32A current since the value at that current is lower than that of 24 A
 - Water contact angle increases with the increase in current but the relation is not linear, That is probably due to measurements error present in the setup. Due to the depth of cut in the workpiece, the base was not visible in the camera, leading to errors. The learnings have been implemented in phase two of the project.
- T_{on} as a varying parameter, values: [25 μ s, 50 μ s, 75 μ s] [$T_{on}+T_{off}=100\mu$ s]
 - MRR increases with an increase in pulse on time while EWR decreases with an increase in pulse on time
 - R_a values first increase and then decrease with the increase in T_{on}
 - R_q values also show a similar trend to that of R_a values
 - S_a Values show a clear increasing trend with the increase in pulse on time

The trends of surface roughness, MRR, EWR, and water contact angle are matching with the trends observed in the literature.

Phase 2: Powder mixed electric discharge machining of SS304 using a copper electrode of diameter 5mm, 0.1mm depth of cut with 20×20mm machined surface area using HAp powder

- Workpiece 1: PMEDM with HAp concentration of 2.5 g/L
- Workpiece 2: EDM without powder keeping the other machining parameters same
- Workpiece 3: PMEDM with reused HAp concentration
 - R_a and R_q measurements of workpiece 1 (with HAp powder) is higher as compared the workpiece 2 (without powder), while the R_a and R_q values of the workpiece machined while reusing the dielectric was found to be the lowest
 - HAp coated surfaces of workpiece 1 and workpiece 3 were found to be hydrophobic in nature since the contact angle is greater than 90 degrees, while the surface of workpiece 2 was found to be hydrophilic in nature.

- Presence of the hydroxyapatite powder was confirmed with FESEM-EDS analysis by getting the Phosphorous and Calcium elements in significant amounts on the surface
- In workpiece 3, the percentage weight of both the elements calcium and phosphorus decreased as compared to that of workpiece 1
- Ca:P ratio was found to be 1.58 in workpiece 1 while it was 1.5 in workpiece which matches the requirements of the ratio for biocompatible materials found in literature [11].

5.2 Future Work

This research can be extended by studying the variation of the texture properties with multiple levels of discharge current, pulse on time and concentration of hydroxyapatite powder. Further, we can add silver powder (Ag) with hydroxyapatite (HAp) in various concentration levels to deposit both of them on the surface. After performing the experiments, more tests can be performed to prove the biocompatibility, such as hardness, corrosion resistance, wear resistance, surface adhesion, in vitro biocompatibility test, and anti-microbial test.

Acknowledgments

We would like to express our sincere appreciation to all the individuals and laboratories that have contributed to the successful completion of this report.

Firstly, we would like to thank Mr. Ratan Ahuja and Mr. Shashank Shukla for their valuable support throughout this project. Their insightful comments and suggestions were instrumental in shaping the direction of this study. The project would not have progressed without their help. Mr. Shashank's expertise and dedication were crucial in getting roughness profile results through ALICONA. We are also grateful to the technician Mr. Arun Nair at the MTL laboratory for their assistance with the W-EDM cutting.

We would like to extend our gratitude to MTL Lab, MMMF Lab, PG Lab chemical department, MEMS Dept, and Mechanical Workshop. Their cooperation and various facilities were essential in making this study possible.

Finally, we would like to acknowledge the support of our colleague Ms. Tanvi Joshi in Phase 1 of the experiment and the initial stages of Phase 2. Our guide professor, Dr. Soham Mujumdar, provided us with guidance and encouragement throughout the entire process. Their feedback and constructive criticism were invaluable in refining our ideas and improving the quality of this report.

Thank you all for your contributions to this project.

References

- [1] Choudhary, Sushil & Jadoun, R & Kumar, Arjun & Ajay,. (2014). Latest Research Trend of optimization Techniques in Electric Discharge Machining (EDM): Review Article. International Journal of Research in Engineering & Advanced Technology. 2. 2320-8791.
- [2] Bui, Viet D., James W. Mwangi, and Andreas Schubert. "Powder mixed electrical discharge machining for antibacterial coating on titanium implant surfaces." *Journal of Manufacturing Processes* 44 (2019): 261-270.
- [3] Ta, D. V., Dunn, A., Wasley, T. J., Kay, R. W., Stringer, J., Smith, P. J., Connaughton, C., & Shephard, J. D. (2015). Nanosecond laser textured superhydrophobic metallic surfaces and their chemical sensing applications. *Applied Surface Science*, 357, 248-254. <https://doi.org/10.1016/j.apsusc.2015.09.027>
- [4] Malshe, A., Rajurkar, K., Samant, A., Hansen, H. N., Bapat, S., & Jiang, W. (2013). Bio-inspired functional surfaces for advanced applications. *CIRP Annals*, 62(2), 607-628.
<https://doi.org/10.1016/j.cirp.2013.05.008>
- [5] Khandizod, R., Varghese, V., & Mujumdar, S. (2022). Electric Discharge Assisted Surface Texturing of Stainless Steel 304. *Procedia CIRP*, 108, 670-674. <https://doi.org/10.1016/j.procir.2022.03.104>
- [6] Aghdeaba, ShukryH, Mohammed M. Hasan, and Ghaith A. Makhribc. "Effect of gap space on surface roughness (Ra) in the electrical discharge machining (EDM) for tool steel AISI M6." *Design Engineering* (2021): 11358-11366.
- [7] Pradhan, M. K., and C. K. Biswas. "Modeling and Analysis of process parameters on Surface Roughness in EDM of AISI D2 tool Steel by RSM Approach." (2009).
- [9] Kiyak, M., & Çakır, O. (2007). Examination of machining parameters on surface roughness in EDM of tool steel. *Journal of Materials Processing Technology*, 191(1-3), 141-144.
<https://doi.org/10.1016/j.jmatprotec.2007.03.008>
- [10] Sandhu, Harpinder Singh, et al. "Investigation of electric discharge machining of Inconel 718 using special graphite electrode." National Conference on Advances in Engineering, Technology & Management, IOSR Journal of Mechanical and Civil Engineering. 2015.
- [11] Al-Amin, Md, et al. "Powder mixed-EDM for potential biomedical applications: A critical review." *Materials and Manufacturing Processes* 35.16 (2020): 1789-1811.
- [12] Lu, Jingyi, Huijun Yu, and Chuanzhong Chen. "Biological properties of calcium phosphate biomaterials for bone repair: A review." *RSC advances* 8.4 (2018): 2015-2033.
- [13] Al-Amin, Md, et al. "Bio-ceramic coatings adhesion and roughness of biomaterials through PM-EDM: a comprehensive review." *Materials and Manufacturing Processes* 35.11 (2020): 1157-1180.

[14] Prakash, Chander, et al. "Electric discharge machining—A potential choice for surface modification of metallic implants for orthopedic applications: A review." *Proceedings of the Institution of Mechanical Engineers, Part B: Journal of Engineering Manufacture* 230.2 (2016): 331-353.

[15] Meshramkar, R., et al. "Surface treatment of zirconia implant, its surface roughness and its effect on osseointegration-a review." *Int J Innov Res Med Sci* 4 (2019): 343-345.

[16] Asri, R., Harun, W., Hassan, M., Ghani, S., & Buyong, Z. (2016). A review of hydroxyapatite-based coating techniques: Sol-gel and electrochemical depositions on biocompatible metals. *Journal of the Mechanical Behavior of Biomedical Materials*, 57, 95-108. <https://doi.org/10.1016/j.jmbbm.2015.11.031>

[17] Kieswetter, K., Schwartz, Z., Dean, D. D., & Boyan, B. D. (1996). The Role of Implant Surface Characteristics in the Healing of Bone. *Critical Reviews in Oral Biology & Medicine*.

<https://doi.org/10.117710454411960070040301>

[18] Drelich, Jaroslaw, and Abraham Marmur. "Physics and applications of superhydrophobic and superhydrophilic surfaces and coatings." *Surface Innovations* 2.4 (2014): 211-227.

[16] Rodriguez-Contreras, A., Guadarrama Bello, D., & Nanci, A. (2018). Surface nanoporosity has a greater influence on osteogenic and bacterial cell adhesion than crystallinity and wettability. *Applied Surface Science*, 445, 255-261. <https://doi.org/10.1016/j.apsusc.2018.03.150>

[17] Pujiyulianto, E., Suyitno Effect of pulse current in manufacturing of cardiovascular stent using EDM die-sinking. *Int J Adv Manuf Technol* 112, 3031–3039 (2021). <https://doi.org/10.1007/s00170-020-06484-3>

[18] Al-Amin, M., Abdul-Rani, A. M., Rana, M., Hastuty, S., Danish, M., Rubaiee, S., & Mahfouz, A. B. (2022). Evaluation of modified 316L surface properties through HAp suspended EDM process for biomedical application. *Surfaces and Interfaces*, 28, 101600. <https://doi.org/10.1016/j.surfin.2021.101600>

Appendix



Fig. 1 machined workpiece in phase 1

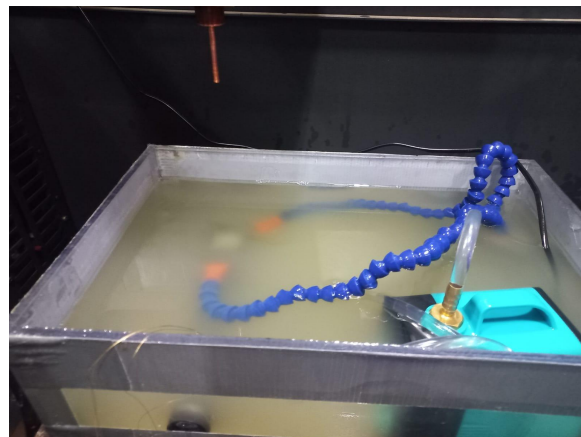


Fig.2 Circulation tank with dielectric-filled (before machining)

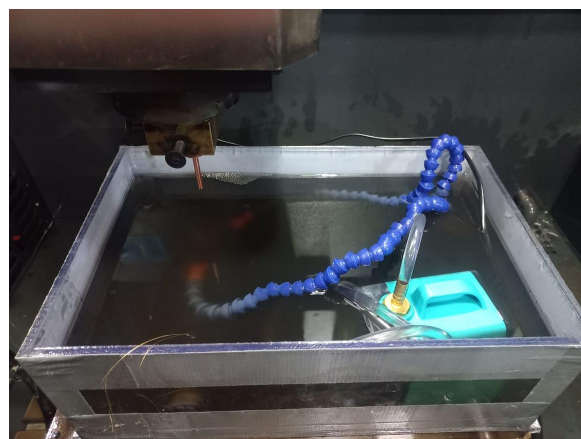
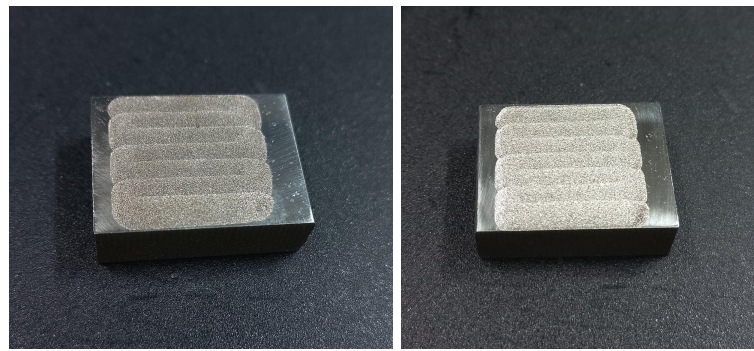


Fig.3 Circulation tank with dielectric-filled (after machining)

An important observation:

As seen in Figures 2 and 3 the dielectric turned black after the machining due to the creation of the debris. As discussed in the report, we reused the dielectric to study the effect of the debris on the deposition of powder.



(a)

(b)

Fig. 4 Machined workpiece a) with powder b) without powder in phase two

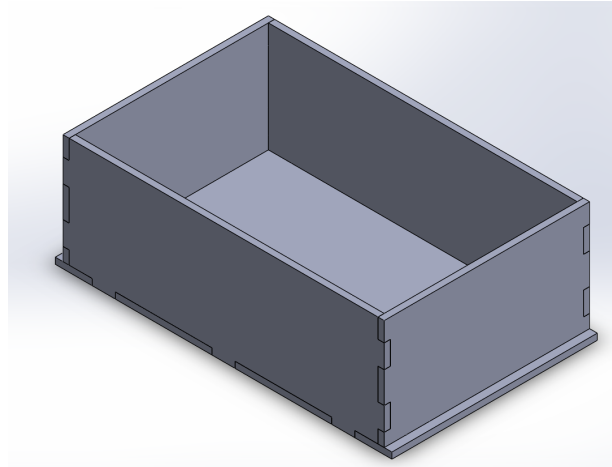
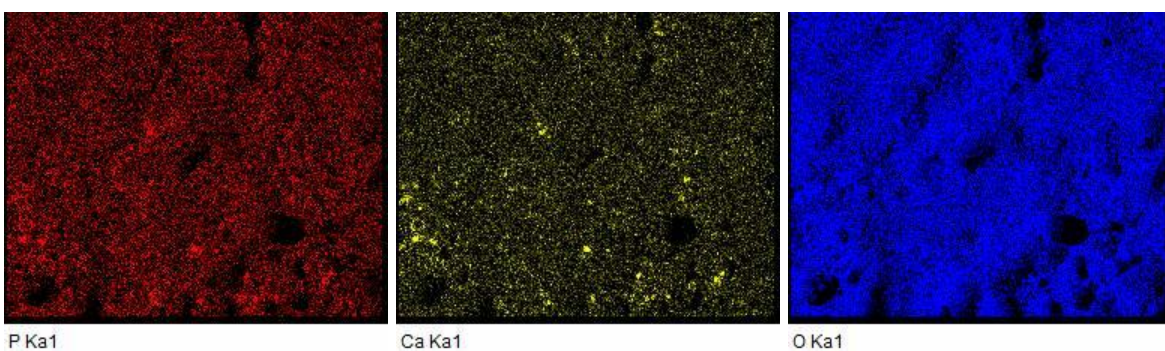
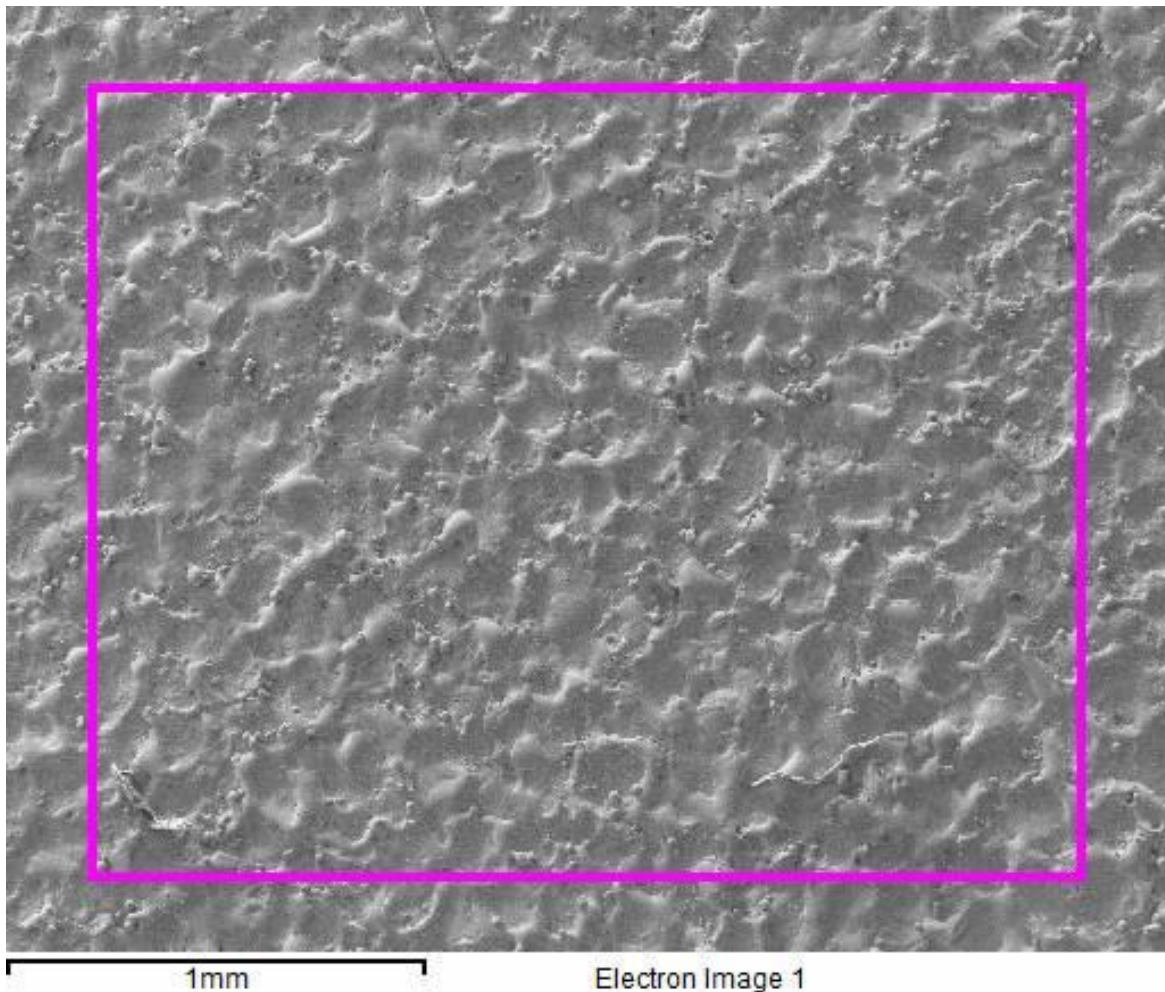


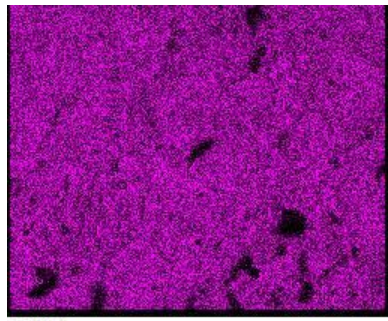
Fig.5 Isometric view of the CAD of the tank (it was made to do the laser cutting)

Elemental mapping tough FESEM-EDS:

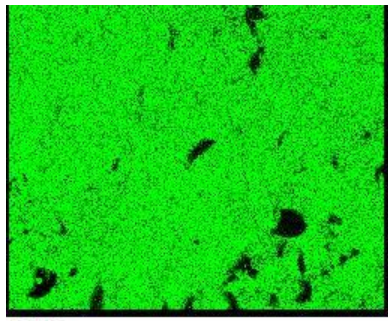
It shows the region in which the particular element is present. The colour intensity represents the amount present at the particular location. Particular element is mention below of every image.

[1] Workpiece 1 (machined with HAp)

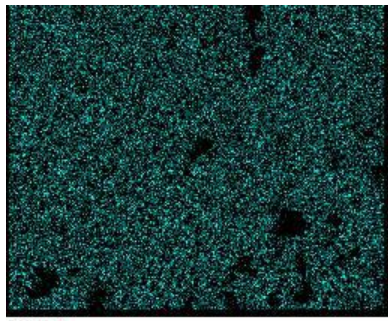




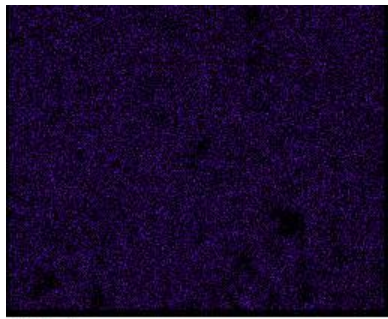
Cr Ka1



Fe Ka1



Ni Ka1



Mn Ka1